© 2023. Published by The Company of Biologists Ltd | Journal of Cell Science (2023) 136, jcs260124. doi:10.1242/jcs.260124

RESEARCH ARTICLE

The fission yeast kinetochore complex Mhf1–Mhf2 regulates the spindle assembly checkpoint and faithful chromosome segregation

Yanze Jian, Lingyun Nie, Sikai Liu, Yueyue Jiang, Zhen Dou, Xing Liu, Xuebiao Yao* and Chuanhai Fu*

ABSTRACT

The outer kinetochore serves as a platform for the initiation of the spindle assembly checkpoint (SAC) and for mediating kinetochore–microtubule attachments. How the inner kinetochore subcomplex CENP-S–CENP-X is involved in regulating the SAC and kinetochore–microtubule attachments has not been well characterized. Using live-cell microscopy and yeast genetics, we found that Mhf1–Mhf2, the CENP-S–CENP-X counterpart in the fission yeast *Schizosaccharomyces pombe*, plays crucial roles in promoting the SAC and regulating chromosome segregation. The absence of Mhf2 attenuates the SAC, impairs the kinetochore localization of most of the components in the constitutive centromere-associated network (CCAN), and alters the localization of the kinase Ark1 (yeast homolog of Aurora B) to the kinetochore. Hence, our findings constitute a model in which Mhf1–Mhf2 ensures faithful chromosome segregation by regulating the accurate organization of the CCAN complex, which is required for promoting SAC signaling and for regulating kinetochore–microtubule attachments.

This article has an associated First Person interview with the first author of the paper.

KEY WORDS: Fission yeast, Kinetochore, Mhf2, Mitosis, Spindle assembly checkpoint

INTRODUCTION

Faithful chromosome segregation requires kinetochores to be assembled in a cell cycle-dependent manner at the centromere of a chromosome (Cheeseman, 2014). During mitosis, kinetochores function to mediate chromosome alignment and segregation by attaching chromosomes to spindle microtubules (Musacchio and Desai, 2017). In addition, kinetochores serve as a platform for signaling of the spindle assembly checkpoint (SAC), a safeguard mechanism governing faithful chromosome segregation (London and Biggins, 2014; Musacchio, 2015).

Kinetochores comprise structural and nonstructural components. Of the structural components, the constitutive centromere-associated network (CCAN) is present in the inner layer of kinetochores, whereas the KNL1–Mis12–Ndc80 (KMN) network resides in the outer layer of kinetochores (Perpelescu and Fukagawa, 2011). In mammals, the CCAN complex is further divided into several subcomplexes: CENP-C (Cnp3 in fission yeast), CENP-T (Cnp20)–CENP-W (Wip1), CENP-S (Mhf1)–CENP-X (Mhf2), CENP-H (Fta3)–CENP-I (Mis6)–CENP-K (Sim4), CENP-L (Fta1)–CENP-M (no counterpart in fission yeast)–CENP-N (Mis15) and CENP-O (Mal2)–CENP-P (Fta2)–CENP-Q (Fta7)–CENP-U (Mis17)–CENP-R (no counterpart in fission yeast) (Hara and Fukagawa, 2017; Musacchio and Desai, 2017). In yeast, most of the CCAN components except CENP-M and CENP-R are conserved (Saitoh et al., 2005). The KMN network consists of the evolutionarily conserved proteins KNL1 (Spc7 in fission yeast), the Mis12 complex and the Ndc80 complex, and functions to mediate attachments between kinetochores and spindle microtubules (Cheeseman et al., 2006). Additionally, the KMN network component KNL1 recruits the Bub1–Bub3 complex to mediate SAC signaling (Sharp-Baker and Chen, 2001). The interaction between KNL1 and the Bub1–Bub3 complex depends on phosphorylation of KNL1 by the evolutionarily conserved kinase Mps1 (Mph1 in fission yeast) (London and Biggins, 2014; Yamagishi et al., 2012). Although significant progress has been made in understanding the roles of the KMN network in regulating the SAC, how the CCAN complex contributes to SAC signaling is not well understood.

The CCAN complex bridges the centromere and the KMN network (Hara and Fukagawa, 2017). Two mechanisms underlie the connection between the CCAN complex and the KMN network. In one of the mechanisms, the CCAN component CENP-C interacts with the Mis12 complex, a KMN component, whereas in the other, the CCAN component CENP-T interacts with the KMN component Ndc80 (Ding et al., 2019; Hori et al., 2013; Rago et al., 2015). The subcomplexes of vertebrate CCAN have been reconstituted with purified proteins *in vitro*, revealing additional interfaces between the CCAN complex and the KMN network (Pesenti et al., 2018; Weir et al., 2016). The molecular organization of CCAN subcomplexes in *Saccharomyces cerevisiae* and humans was recently demonstrated by cryo-electron microscopy (Pesenti et al., 2022; Tian et al., 2022; Yan et al., 2019; Yatskevich et al., 2022). There have been few studies on the role of CCAN in SAC signaling. However, it was reported that CENP-I/Mis6 is required for the proper localization of Mad2, a core component of the SAC, to kinetochores in vertebrate and fission yeast cells (Liu et al., 2003; Saitoh et al., 2005). Intriguingly, conditional mutation of *mis6* impairs SAC in fission yeast and depletion of CENP-I arrests mitosis in humans (Saitoh et al., 2005). These findings suggest an association between the CCAN complex and SAC.

The histone fold-containing complex CENP-S–CENP-X (or CENP-S/X) forms a heterotetrameric nucleosome-like structure with CENP-T/W at the centromere (Nishino et al., 2012) and

MOE Key Laboratory for Cellular Dynamics & School of Life Sciences, Division of Life Sciences and Medicine, University of Science and Technology of China, Hefei, China 230027.

*Authors for correspondence (chuanhai@ustc.edu.cn; yaoxb@ustc.edu.cn)

X.Y., 0000-0001-8982-5911; C.F., 0000-0003-4354-3796

Handling Editor: David Glover
Received 12 April 2022; Accepted 13 December 2022

Journal of Cell Science (2023) 136, jcs260124. doi:10.1242/jcs.260124

interacts with FANCM to regulate DNA damage repair and centromere localization (Tao et al., 2012; Yan et al., 2010). Depletion of CENP-S/X increases the distance between inner and outer kinetochores in chicken DT40 cells, and knockdown of CENP-S/X causes defective chromosome segregation in chicken DT40 and HeLa cells (Amano et al., 2009). These findings indicate that CENP-S/X might play roles in CCAN organization and chromosome segregation. Intriguingly, centromere drift occurs frequently in CENP-S-deficient chicken DT40 cells (Hori et al., 2017), and centromere repositioning takes place in fission yeast cells lacking *mhf1* or *mhf2* (Lu and He, 2019). How CENP-S/X contributes to chromosome alignment and segregation remains elusive.

In addition to the SAC, the kinase Aurora B (Ark1 in fission yeast) is required for faithful chromosome segregation. Aurora B phosphorylates Ndc80 to decrease the affinity of Ndc80 to microtubules, by which erroneous attachments between kinetochores and microtubules can be corrected (Welburn et al., 2010). Whether CENP-S/X contributes to chromosome alignment and segregation by regulating Aurora B has not been tested.

The fission yeast *Schizosaccharomyces pombe* has proven to be an excellent model organism to study mitosis and the cell cycle (Hayles and Nurse, 2018). In this work, we found that the absence of Mhf2 attenuated the SAC and caused lagging chromosomes, underscoring the crucial role of Mhf2 in regulating the SAC and chromosome segregation.

RESULTS

The absence of *mhf2* attenuates the SAC and impairs Bub1 localization during mitosis

To determine whether Mhf2 regulates the SAC, we first assessed the efficiency of mitotic arrest of wild-type (WT), *mhf2*-deleted (*mhf2*Δ) and *bub1*-deleted (*bub1*Δ) cells carrying the cold-sensitive *nda3-KM311* allele. The *nda3-KM311* strains can be efficiently arrested at preanaphase after incubation at 16°C (Hagan et al., 2016; Hiraoka et al., 1984; Yamagishi et al., 2012). For the convenience of counting preanaphase cells, we used Plo1–GFP as a proxy (Mulvihill et al., 1999). As shown in Fig. 1A,B, the percentage of mitotic WT cells displaying Plo1–GFP signals increased over time upon incubation at 16°C and, 8 h after cold treatment, ∼90% of WT cells were arrested at preanaphase, presumably due to the activation of the SAC. As Bub1 is a core component of the SAC (Fischer et al., 2021), the absence of Bub1 was expected to abolish the SAC. Consistently, the percentage of mitotic *bub1*Δ cells remained low (<10%) throughout the period of cold treatment (Fig. 1A,B). Intriguingly, similar to the percentage of mitotic WT cells, the percentage of mitotic *mhf2*Δ cells increased over time upon cold treatment, but to a lesser degree (Fig. 1A,B). In addition, the absence of Mhf2 resulted in loss of minichromosome Ch16 (Fig. S1). These results indicate that Mhf2 plays a role in regulating the SAC. The effect of the deletion of *mhf2* on the SAC did not appear to be caused indirectly by the altered expression of the neighboring genes of *mhf2* because real-time quantitative PCR (RT-qPCR) experiments showed that the expression levels of these genes were comparable between *mhf2*+ and *mhf2*Δ cells (Fig. S2).

We next examined the effect of the absence of Mhf2 on the localization of Bub1 by live-cell microscopy. We observed 40 mitotic *mhf2*+ and 43 mitotic *mhf2*Δ cells (Fig. 1C). Most of the observed cells completed mitosis within 20 min but three *mhf2*Δ cells failed to exit mitosis after 60 min (Fig. 1C). Therefore, for comparison of Bub1–GFP signals throughout mitosis, only cells capable of completing mitosis were selected for determining the average Bub1–GFP signal intensity along the spindle at all time points when stack images were acquired. As shown in Fig. 1D, the intensity of Bub1–GFP increased at the beginning of mitosis and decreased gradually later (2–3 min after entering mitosis). Intriguingly, the Bub1–GFP signal intensity was generally weaker in *mhf2*Δ cells than in *mhf2*+ cells, despite comparable expression levels of Bub1–GFP detected in *mhf2*+ and *mhf2*Δ cells (Fig. 1D,E). These results indicate that Mhf2 might regulate the SAC by modulating the localization of Bub1 to kinetochores during mitosis.

Epistasis analysis further revealed that the absence of both Bub1 and Mhf2 caused slow growth on a yeast extract medium (YE) plate and that the absence of both Bub1 (or Mad2) and Mhf2 had an additive effect on the growth of cells cultured on YE plates containing the microtubule depolymerizing drug methyl-2-benzimidazole-carbamate (MBC) (Fig. S3). These phenotypes might be due to the effects of the absence of Mhf2 on both the SAC and kinetochore organization (see below).

Mhf2 is required for the localization of Bub1 and Spc7 to kinetochores at preanaphase

To further test the localization of Bub1 to the kinetochore, we created *mhf2*+ and *mhf2*Δ cells expressing Bub1–GFP and Cnp3–tdTomato (marking kinetochores) and carrying the *nda3-KM311* allele. Microscopy images acquired after the cells were cultured at 16°C for 6 h showed different localization patterns of Bub1–GFP and Cnp3–tdTomato (Fig. 2A,B). Quantification showed that Bub1–GFP and Cnp3–tdTomato completely colocalized in ∼92% of *mhf2*+ cells (type II pattern, as indicated in Fig. 2A) versus ∼51% of *mhf2*Δ cells, Bub1–GFP and Cnp3–tdTomato partly colocalized in ∼6% of *mhf2*+ cells (type III pattern) versus ∼27% of *mhf2*Δ cells, and Bub1–GFP was absent from all Cnp3–tdTomato foci in ∼1% of *mhf2*+ cells (type IV pattern) versus ∼22% of *mhf2*Δ cells (Fig. 2C). In addition, additional Bub1–GFP foci that did not colocalize with Cnp3–tdTomato were present in ∼1% of *mhf2*Δ cells (type V pattern; Fig. 2C). We further compared the average intensity of Bub1–GFP in type II *mhf2*+ and *mhf2*Δ cells, revealing that the Bub1–GFP signal intensity was significantly weaker on the kinetochore in *mhf2*Δ cells than in *mhf2*+ cells (Fig. 2D). The altered localization of Bub1–GFP was not due to altered expression of Bub1–GFP as comparable expression of Bub1–GFP was detected in *mhf2*+ and *mhf2*Δ cells (Fig. 2E). Similar results were found when we examined the localization of Mad2–GFP in *mhf2*+, *mhf2*Δ and *bub1*Δ cells (Fig. S4). Thus, we concluded that Mhf2 plays a crucial role in promoting the localization of Bub1 and Mad2 to kinetochores.

It has been shown that Mph1/Mps1-mediated phosphorylation of Spc7 (the counterpart of human KNL1 in fission yeast) is required for the recruitment of the Bub1–Bub3 complex to kinetochores (Yamagishi et al., 2012). Therefore, we similarly assessed the localization of Spc7–GFP by using *mhf2*+ and *mhf2*Δ cells expressing Spc7–GFP and Cnp3–tdTomato and carrying the *nda3-KM311* allele (Fig. 2F). Similar to interphase cells, some mitotic cells also displayed only one Spc7–GFP- and Cnp3–tdTomato-containing punctum. Therefore, it was impossible to distinguish the cell cycle phase of these cells. For quantification, we counted only cells containing multiple Cnp3–tdTomato foci. The quantification result for Spc7–GFP localization was similar to that for Bub1–GFP localization (Fig. 2G,H). Given the low expression of Spc7 within the cell, we failed to detect Spc7–GFP using cell lysates by western blotting assays. Therefore, we performed an immunoprecipitation assay to enrich Spc7–GFP from *mhf2*+ and *mhf2*Δ cells, and the results showed that the expression levels of Spc7–GFP from *mhf2*+ and *mhf2*Δ cells were comparable (Fig. 2I).

Journal of Cell Science (2023) 136, jcs260124. doi:10.1242/jcs.260124

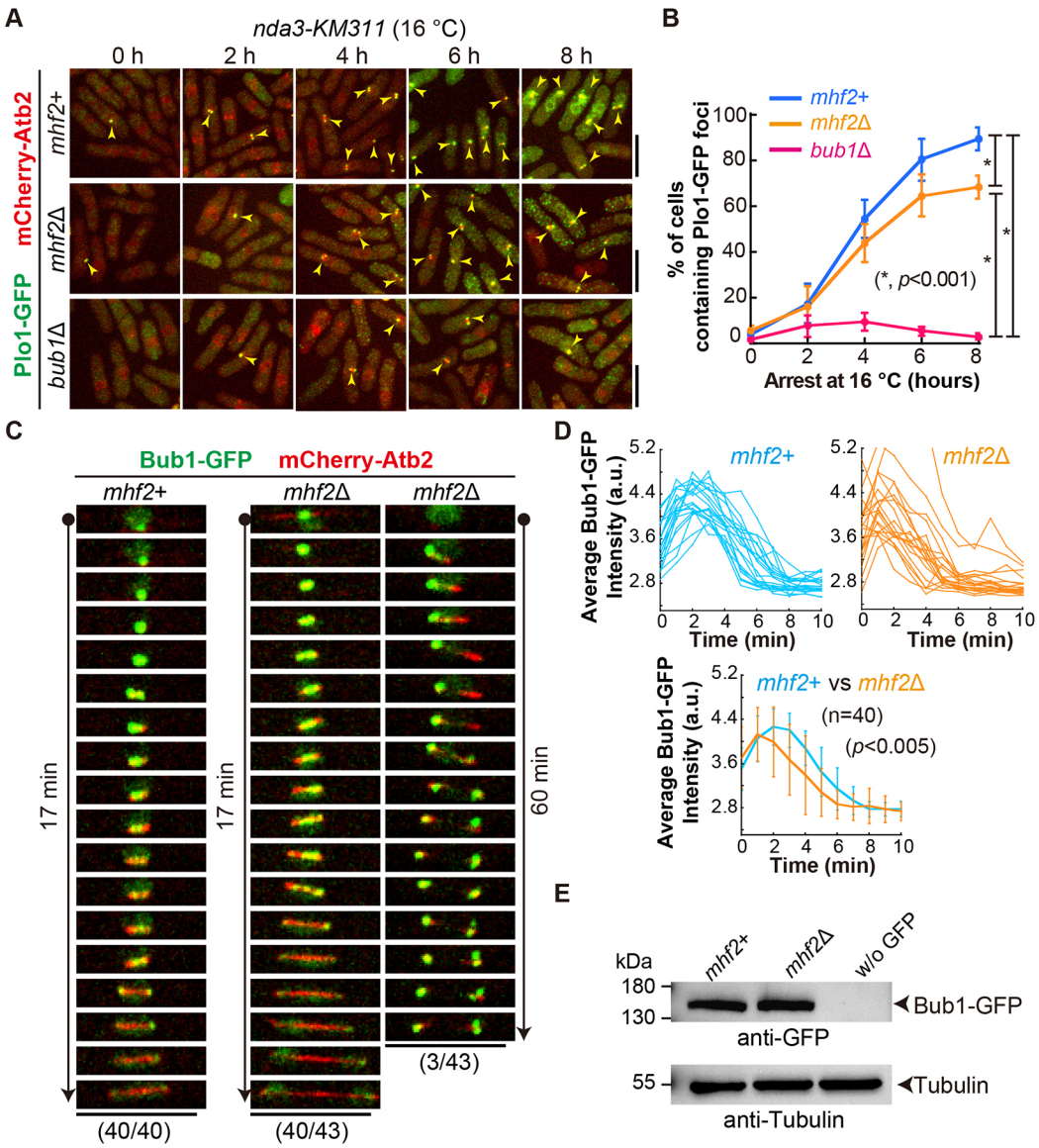

Fig. 1. The absence of Mhf2 impairs the spindle assembly checkpoint and the localization of Bub1. (A) Maximum-projection images of WT (*mhf2*+), *mhf2*-deleted (*mhf2Δ*) and *bub1Δ* cells expressing Plo1–GFP and mCherry–Atb2 (α-tubulin) and carrying the *nda3-KM311* allele. Cells were cultured at the restrictive temperature (16°C), and images were acquired every 2 h. Arrowheads indicate Plo1–GFP in cells at preanaphase. Note that the spindle was broken down at the restrictive temperature. Scale bars: 10 µm. (B) Quantification of the percentage of cells containing Plo1–GFP foci indicated in A. Error bars represent s.d., and *P*-values were calculated by two-way ANOVA. More than 750 cells per time point and sample were analyzed, and five independent experiments were performed. (C) Maximum-projection time-lapse images of *mhf2*+ and *mhf2Δ* cells expressing Bub1–GFP and mCherry–Atb2. Note that three cells did not exit mitosis. Scale bar: 10 µm. (D) Plots of the average Bub1–GFP intensity along the spindle over time. Time zero is the onset of mitosis. The top graphs show measurements for individual cells (40 *mhf2*+ and *mhf2Δ* cells were analyzed) and the bottom graph is the summarized graph, in which the thick lines represent the average Bub1–GFP intensity of the 40 cells at each time point and error bars represent s.d. The *P*-value was calculated by two-way ANOVA. Two independent experiments were performed and similar results were obtained. a.u., arbitrary units. (E) Western blotting analysis was performed to test the expression of Bub1–GFP in *mhf2*+ and *mhf2Δ* cells with antibodies against GFP and tubulin. 'w/o' indicates a WT strain that did not carry a GFP fusion protein. Images are representative of two independent experiments.

Collectively, these results support the conclusion that Mhf2 plays a crucial role in regulating the localization of both Spc7 and Bub1 to the kinetochores during mitosis.

The absence of *mhf2* impairs the localization of the CCAN and KMN components to the kinetochores

How does Mhf2, a protein in the inner kinetochore, affect Bub1 and Spc7, two proteins in the outer kinetochore? We reasoned that Mhf2 might be required for the proper organization of the CCAN and KMN complexes. The absence of Mhf2 might impair the localization of Bub1 to the kinetochores by disorganization of the CCAN and KMN network. To test this hypothesis, we used live-cell microscopy to compare the localization of CCAN and KMN proteins on kinetochores in *mhf2*+ and *mhf2Δ* cells. A method allowing for simultaneous observation of *mhf2*+ and *mhf2Δ* cells was developed to ensure the high reliability of the comparison data. Briefly, to distinguish *mhf2Δ* from *mhf2*+ cells, *mhf2*+ cells were stained with lectin (marking cell membranes) and then mixed with *mhf2Δ* cells for simultaneous imaging, followed by measurements of average fluorescence intensity on kinetochores with the same

Journal of Cell Science (2023) 136, jcs260124. doi:10.1242/jcs.260124

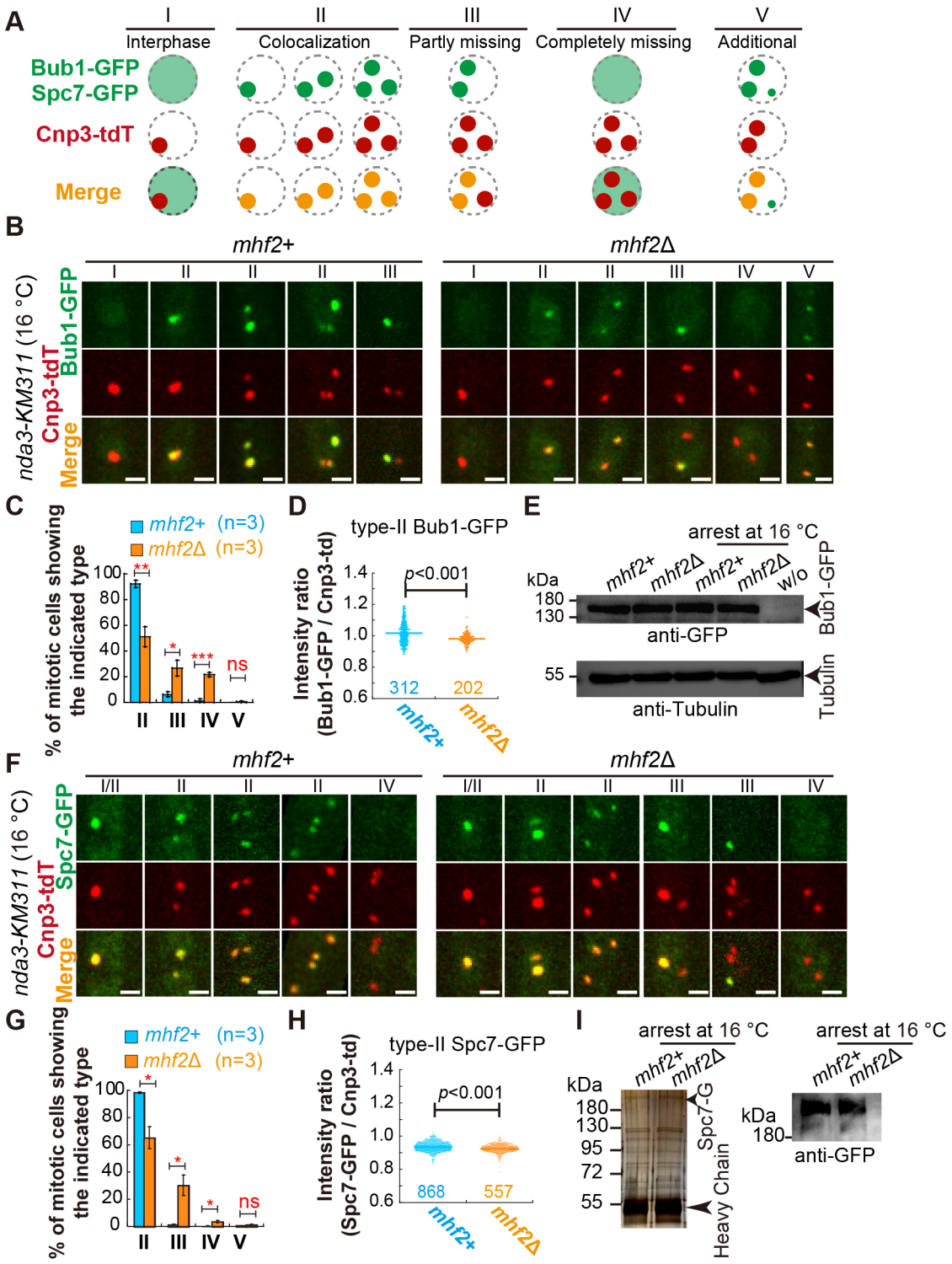

Fig. 2. See next page for legend.

microscopy image (Fig. 3A). It has been reported that Mhf1 and Mhf2 form a tetramer and localize to the kinetochores interdependently (Amano et al., 2009; Nishino et al., 2012). Consistently, by using the above imaging method, we clearly observed that the localization of Mhf1 to the kinetochores was almost abolished in *mhf2*Δ cells (Fig. 3B). Similarly, the localization of almost all CCAN components, including Cnp3 (CENP-C in humans), Fta1 (CENP-L), Mis15 (CENP-N), Fta3 (CENP-H), Mis6 (CENP-I), Sim4 (CENP-K), Mal2 (CENP-O), Fta2 (CENP-P) and Fta7 (CENP-Q), to the kinetochores was impaired by the absence of Mhf2 (Fig. 3C–F). In addition, we observed that the localization of the KMN components Spc7, Mis12 and Ndc80 to the kinetochores was impaired in *mhf2*Δ cells (Fig. 3G,H, Fig. 4A,C). Intriguingly, the localization of the centromere-specific histone variant Cnp1 (CENP-A) was not altered by the absence of Mhf2 (Fig. 3B). Surprisingly, the

Journal of Cell Science (2023) 136, jcs260124. doi:10.1242/jcs.260124

Fig. 2. Mhf2 is required for the proper localization of Bub1 and Spc7 to kinetochores. (A) Schematic diagram illustrating the localization patterns of Bub1–GFP, Spc7–GFP and Cnp3–tdTomato (Cnp3-tdT) at interphase (type I) and preanaphase (types II–V). At interphase, Bub1–GFP diffuses within the nucleus, whereas Spc7–GFP displays as one punctum. Types II and III indicate complete and partial colocalization of Bub1–GFP and Spc7–GFP with Cnp3–tdTomato, respectively; type IV indicates no localization of Bub1–GFP on kinetochores; and type V indicates the presence of an additional Bub1–GFP punctum that does not colocalize with Cnp3–tdTomato. (B) Representative maximum-projection images of *mhf2*+ and *mhf2*Δ cells expressing Bub1–GFP and Cnp3–tdTomato and carrying the *nda3-KM311* allele. For mitotic arrest, cells were cultured at 16°C for 6 h. The Roman numerals indicate the type of Bub1–GFP localization as shown in A. Scale bars: 2 µm. (C) Quantification of the Bub1–GFP localization patterns indicated in A. A total of 244 *mhf2*+ and 234 *mhf2*Δ cells from three independent experiments were analyzed. Statistical analysis was performed by two-tailed unpaired Student's *t*-test (ns, not significant; **P*<0.05; ***P*<0.01; ****P*<0.001). Error bars represent s.d. (D) Measurements of the average intensity of Bub1–GFP in type II *mhf2*+ and *mhf2*Δ cells. The *P*-value was calculated by two-tailed unpaired Student's *t*-test, and the number of cells analyzed is indicated. Three independent experiments were performed. (E) Western blotting analysis was performed to test the expression of Bub1–GFP in the indicated cells. Note that cells were cultured at the permissive temperature (30°C) or at the restrictive temperature (16°C). 'w/o' indicates a WT strain that did not carry GFP fusion proteins. Antibodies against GFP and tubulin were used. (F) Representative maximum-projection images of *mhf2*+ and *mhf2*Δ cells expressing Spc7–GFP and Cnp3–tdTomato and carrying the *nda3-KM311* allele. For mitotic arrest, cells were cultured at 16°C for 6 h. Spc7–GFP displayed one punctum in interphase, making it impossible to distinguish mitotic cells that also displayed one Spc7–GFP punctum. Therefore, cells containing ≥2 Spc7–GFP puncta were used for quantification. The Roman numerals indicate the type of Spc7–GFP localization as shown in A. Scale bars: 2 µm. (G) Quantification of the Spc7–GFP localization patterns indicated in A. A total of 342 and *mhf2*+ and 390 *mhf2*Δ cells from three independent experiments were analyzed. Statistical analysis was performed by two-tailed unpaired Student's *t*-test independently (ns, not significant; **P*<0.05). Error bars represent s.d. (H) Measurements of Spc7–GFP average intensity in type II *mhf2*+ and *mhf2*Δ cells. The *P*-value was calculated by two-tailed unpaired Student's *t*-test, and the cell number analyzed is indicated. Three independent experiments were performed. (I) SDS-PAGE (left) and western blotting (right) analysis of immunoprecipitated Spc7–GFP from *nda3-KM311 mhf2*+ and *nda3-KM311 mhf2*Δ cells that were arrested at 16°C. Images are representative of two independent experiments.

localization of Cnp20 (CENP-T) to kinetochores was enhanced significantly in *mhf2*Δ cells (Fig. 3C). Collectively, these data support the model that Mhf2 is required for the proper localization of CCAN and KMN components to the kinetochores (Fig. 3H).

Proper localization of Spc7 and Ndc80 to the kinetochores depends on the CCAN

The KMN network is present in the outer kinetochore (DeLuca et al., 2005) and Spc7 (KNL1) in the KMN network initiates SAC signaling by recruiting the Bub1–Bub3 complex, whereas Ndc80 in the KMN network mediates microtubule–kinetochore attachments (Musacchio and Desai, 2017). As Mhf2 is involved in organizing the CCAN complex (demonstrated above) and multiple interfaces are present between the CCAN and KMN network (Pesenti et al., 2018; Weir et al., 2016), we determined whether the CCAN subcomplexes are required for directing the proper localization of Spc7 and Ndc80 to the kinetochores. Using a similar imaging approach as shown above, we first examined Spc7 localization in WT and *cnp20* (CENP-T in humans, representing the CENP-T/W subcomplex), *mis15* (CENP-N in humans, representing the CENP-L/N subcomplex), *mis6* (CENP-I in humans, representing the CENP-H/I/K subcomplex), and *mis17* (CENP-U in humans, representing the CENP-O/P/Q/U subcomplex) conditional mutant cells. As shown in Fig. 4A,B, the localization of Spc7 to the kinetochores was impaired in *mis15* and *mis6* cells, but not in *cnp20* and *mis17* cells at the restrictive temperature of 37°C (Fig. 4A,B). These results suggest that the CCAN subcomplexes Fta1–Mis15 and Fta3–Mis6–Sim4 play a crucial role in mediating the localization of Spc7 to the outer kinetochore.

A similar approach as above was used to examine the kinetochore localization of Ndc80. As shown in Fig. 4C,D, in addition to the previously reported role of Cnp20 (Huis In 't Veld et al., 2016), the CCAN subcomplexes Fta1–Mis15, Fta3–Mis6–Sim4 and Mal2–Fta2–Fta7–Mis17 also play an important role in mediating the localization of Ndc80 to the outer kinetochore. Hence, synergism between the CCAN subcomplexes is required for promoting the localization of Spc7 and Ndc80 to the outer kinetochore.

The absence of Mhf2 impairs the localization of Ark1 to kinetochores

The kinase Aurora B (Ark1 in fission yeast) functions to correct kinetochore–microtubule attachments by phosphorylating Ndc80 (Welburn et al., 2010). Therefore, we examined the localization of Ark1 to the kinetochore at preanaphase in *mhf2*+ *and mhf2*Δ cells carrying the *nda3-KM311* allele (Fig. 5A). Quantification showed that Ark1–GFP and Cnp3–tdTomato completely colocalized in ∼93% of *mhf2*+ cells (type II pattern) versus ∼72% of *mhf2*Δ cells, Ark1–GFP and Cnp3–tdTomato partly colocalized in ∼4% of *mhf2*+ cells (type III pattern) versus ∼12% of *mhf2*Δ cells, and Ark1–GFP was absent from all Cnp3–tdTomato foci in ∼2% of *mhf2*+ cells (type IV pattern) versus ∼11% of *mhf2*Δ cells (Fig. 5A,B). In addition, Ark1–GFP foci did not colocalize with Cnp3–tdTomato in ∼4% *mhf2*Δ cells (type V pattern; Fig. 5A). We further measured the average Ark1–GFP intensity on kinetochores in type II *mhf2*+ and *mhf2*Δ cells and found that the Ark1–GFP intensity was significantly higher on kinetochores in *mhf2*Δ cells than in *mhf2*+ cells (Fig. 5C). The altered Ark1–GFP localization was not due to altered expression of Ark1–GFP (Fig. 5D).

To monitor the dynamic localization of Ark1–GFP during mitosis, we observed Ark1–GFP and mCherry–Atb2 (marking microtubules) simultaneously by live-cell microscopy (Fig. 5E). Similar to the data presented in Fig. 1C, three *mhf2*Δ cells failed to exist mitosis (Fig. 5E) and, therefore, we did not include these three cells for intensity measurements. Based on the live-cell images, we then measured the average Ark1–GFP signal intensity along the spindle (Ark1 localizes to the kinetochores during preanaphase and all kinetochores are aligned along the spindle) at each time point for *mhf2*+, *mhf2*Δ and *bub1*Δ cells. It has been reported previously that centromeric localization of Aurora B depends on Bub1-mediated phosphorylation of the histone H2A and haspin-mediated phosphorylation of the histone H3 in human cells (Liang et al., 2020; Liu et al., 2015; Watanabe, 2010; Yamagishi et al., 2010). Consistently, we detected the lowest Ark1–GFP signals on the spindle during preanaphase in *bub1*Δ cells (Fig. 5F). Intriguingly, the average Ark1–GFP signals along the spindle were generally higher in *mhf2*Δ cells than in *mhf2*+ cells (Fig. 5F). Taken together, we concluded that Mhf2 is required for promoting the proper localization of Ark1 to the kinetochores.

Mhf2 is required for faithful chromosome segregation and proper kinetochore–microtubule attachments

Finally, we carried out live-cell imaging to examine kinetochore dynamics in *mhf2*+, *mhf2*Δ, and *bub1*Δ cells. As shown in Fig. 6A, 31% of *mhf2*Δ cells (*n*=48) and 35% of *bub1*Δ cells (*n*=59) displayed lagging chromosomes in anaphase B, compared to only

Journal of Cell Science (2023) 136, jcs260124. doi:10.1242/jcs.260124

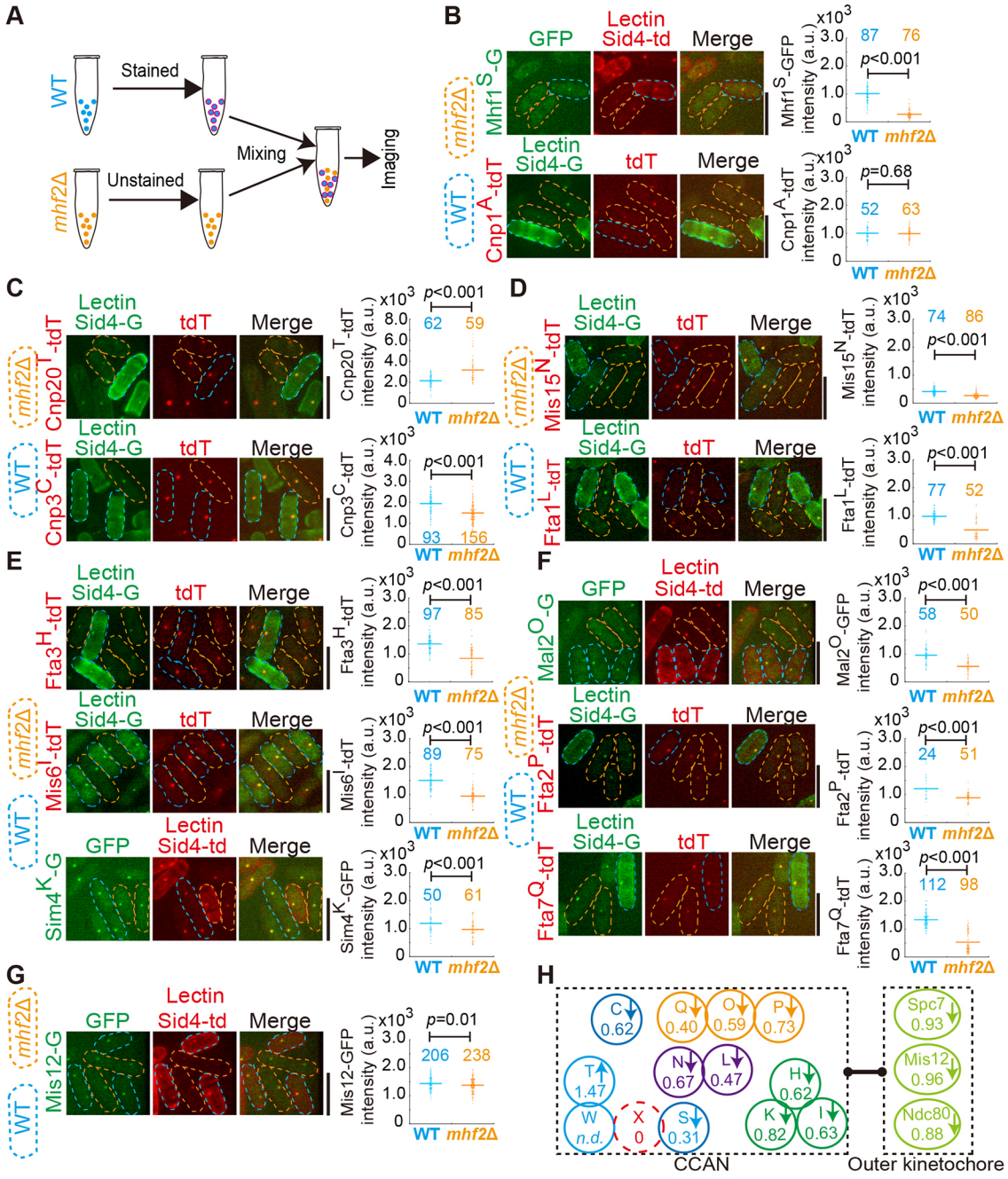

Fig. 3. The absence of Mhf2 impairs the kinetochore localization of Mhf1, Mis12, Cnp3, Fta1, Mis15, Fta3, Mis6, Mal2, Fta2, Fta7 and Sim4, but not Cnp1 and Cnp20. (A) Schematic illustrating the approach used for simultaneous observation of the indicated fusion kinetochore proteins in *mhf2*+ and *mhf2*Δ cells. The stained *mhf2*+ cells were mixed with *mhf2*Δ cells and then analyzed by live-cell microscopy (lectin was used to stain cell membranes). (B–G) Sum-projection images of *mhf2*+ (WT; indicated by blue dashed lines) and *mhf2*Δ (indicated by yellow dashed lines) cells expressing the indicated GFP- or tdTomato-fused proteins. The superscripted letter on the protein name indicates the corresponding human CCAN homolog (CENP). Sid4–GFP and Sid4–tdTomato mark the spindle pole body, and lectin marks the cell membranes only for *mhf2*+ cells. The quantification of the average intensity of the indicated GFP ('G')- or tdTomato ('tdT')-fused proteins is shown on the right. The number of cells analyzed is indicated, and the *P*-values were calculated by two-tailed unpaired Student's *t*-test. a.u., arbitrary units. Scale bars: 10 µm. (H) Schematic diagram summarizing the results shown in B–G (the data for Spc7 and Ndc80 are shown in Fig. 4A,C). The letters indicate the names of the human kinetochore CCAN component (CENP). Upwards and downwards arrows indicate an increase and decrease in the signal intensity of the indicated protein in *mhf2*Δ cells, respectively, and the numbers show the fold change of the signal intensity (versus WT). n.d., not determined.

8% of *mhf2*+ cells (n=68) (quantification at the timepoint when the spindle length reached 3 µm). To monitor the development of lagging chromosomes, we also quantified the percentage of cells displaying lagging chromosomes at different spindle lengths (Fig. 6B). The results showed that almost no *mhf2*+ cells displayed lagging chromosomes after the spindle length reached 4 µm, whereas many *mhf2*Δ and *bub1*Δ cells still displayed lagging chromosomes as anaphase B progressed (Fig. 6B).

As Ark1 localizes to the spindle midzone at anaphase B onset (Petersen et al., 2001), we expressed Ark1–GFP in *nda3-KM311*

Journal of Cell Science (2023) 136, jcs260124. doi:10.1242/jcs.260124

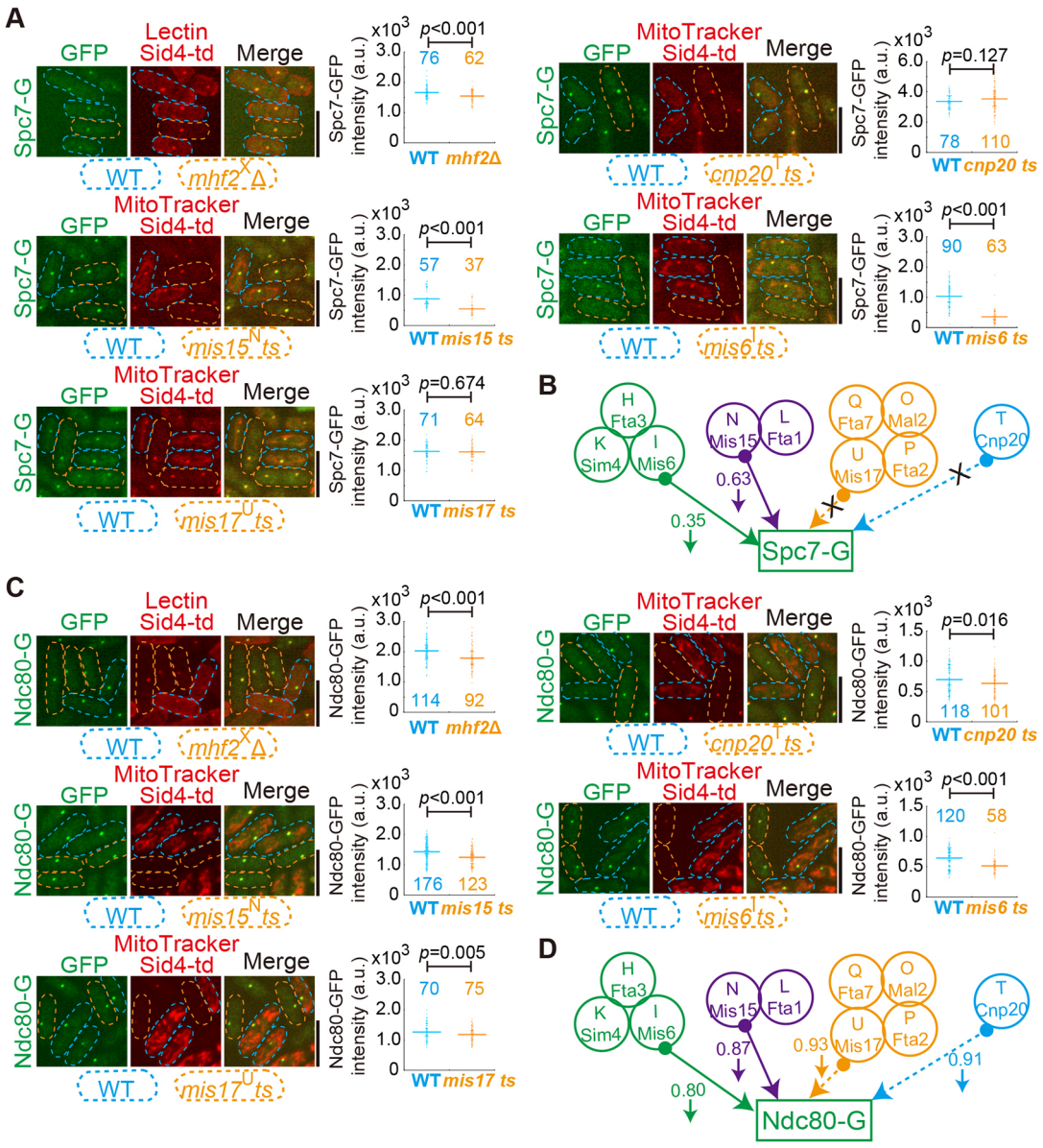

Fig. 4. The kinetochore localization of Spc7 and Ndc80 depends on CCAN subcomplexes. (A) Sum-projection images of the indicated cells [i.e. WT (*mhf2*+), *mhf2*Δ, *cnp20* ts, *mis15* ts, *mis6* ts and *mis17* ts ('ts' represents temperature-sensitive)] expressing Spc7–GFP and Sid4–tdTomato. Cells were cultured at the restrictive temperature of 37°C for 2 h and then examined by live-cell imaging. The superscripted letter on the gene name indicates the corresponding human CCAN homolog (CENP). MitoTracker and lectin mark only *mhf2*+ cells, and the blue and yellow dashed lines indicate *mhf2*+ and mutant cells, respectively. The quantification of the average intensity of Spc7–GFP is shown on the right. The number of cells analyzed is indicated, and the *P*-values were calculated by two-tailed unpaired Student's *t*-test. Scale bars: 10 µm. (B) Schematic diagram summarizing the results shown in A. Solid lines indicate a dependent relationship for the localization of Spc7 to kinetochores and dashed lines with a cross indicate an independent relationship. The number shows the fold change of the signal intensity (versus WT). (C) Sum-projection images of the indicated cells [WT (*mhf2*+), *mhf2*Δ, *cnp20* ts, *mis15* ts, *mis6* ts and *mis17* ts] expressing Ndc80–GFP and Sid4–tdTomato. Cells were cultured at the restrictive temperature of 37°C for 2 h and then examined by live-cell imaging. The superscripted letter on the gene name indicates the corresponding human CCAN homolog (CENP). MitoTracker and lectin mark only *mhf2*+ cells, and the blue and yellow dashed lines indicate *mhf2*+ and mutant cells, respectively. The quantification of the average intensity of Ndc80–GFP is shown on the right. The number of cells analyzed is indicated and *P*-values were calculated by two-tailed unpaired Student's *t*-test. Scale bars: 10 µm. (D) Schematic diagram summarizing the results obtained in C. Solid lines indicate a dependent relationship for the localization of Ndc80 to kinetochores. The number shows the fold change of the signal intensity (versus WT). a.u., arbitrary units.

cells to indicate the onset of anaphase B. Mitotic spindles are broken down when the *nda3-KM311* cells are cultured at the restrictive temperature of 16°C and are reestablished when the *nda3-KM311* cells are cultured at the permissive temperature of 30°C (Hiraoka et al., 1984). The spindle reestablishment allows kinetochores to be recaptured and segregated, and, consequently, mitosis resumes. Therefore, we followed the above procedure of cold treatment and release to observe kinetochore (marked by Cnp3–tdTomato) dynamics. As shown in Fig. 6C,D, 75% of *mhf2*+ cells (versus 36.8% of *mhf2*Δ cells) displayed normal chromosome segregation during anaphase B, 15% of *mhf2*+ cells (versus 28.9% of *mhf2*Δ cells) displayed lagging chromosomes during anaphase B and 10% of *mhf2*+ cells (versus 34.2% of *mhf2*Δ cells) displayed unsegregated chromosomes during anaphase, presumably due to

Journal of Cell Science (2023) 136, jcs260124. doi:10.1242/jcs.260124

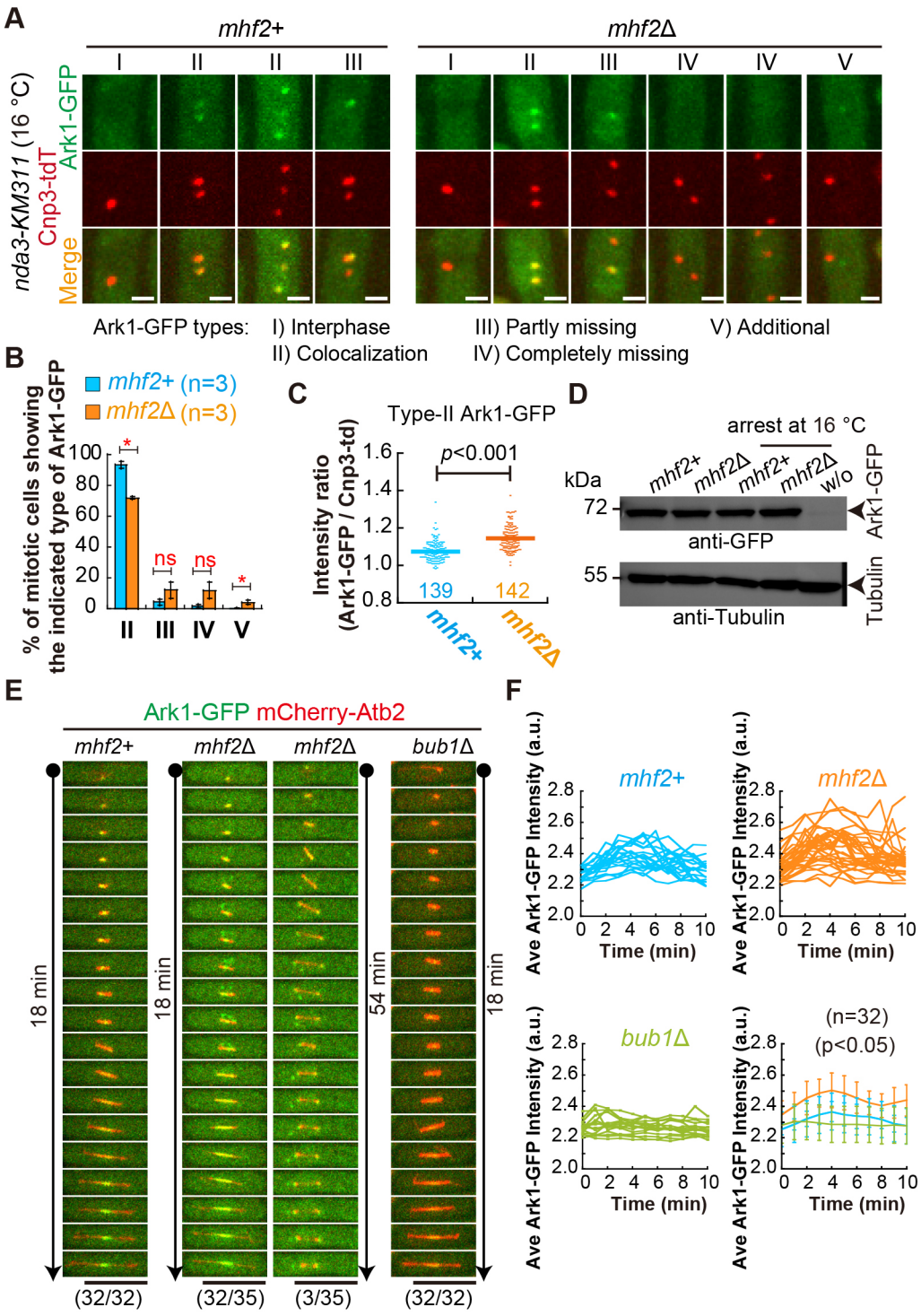

Fig. 5. The absence of Mhf2 affects the proper localization of Ark1 to kinetochores. (A) Representative maximum-projection images of *mhf2*+ and *mhf2*Δ cells expressing Ark1–GFP and Cnp3–tdTomato and carrying the *nda3-KM311* allele. For mitotic arrest, cells were cultured at 16°C for 6 h. The Roman numerals indicate the type of Ark1–GFP localization as shown in Fig. 2A. Scale bars: 2 µm. (B) Quantification of the Ark1–GFP localization patterns indicated in A. A total of 253 and *mhf2*+ and 389 *mhf2*Δ cells from three independent experiments were analyzed. Statistical analysis was performed by two-tailed unpaired Student's *t*-test (ns, not significant; **P*<0.05). Error bars represent s.d. (C) Measurements of the Ark1–GFP average intensity in type II *mhf2*+ and *mhf2*Δ cells. The *P*-value was calculated by two-tailed unpaired Student's *t*-test, and the number of cells analyzed is indicated. Three independent experiments were performed. (D) Western blotting analysis was performed to test the expression of Ark1–GFP in the indicated cells. Note that cells were cultured at the permissive temperature (30°C) or the restrictive temperature (16°C). 'w/o' indicates a WT strain that did not carry GFP fusion proteins. Antibodies against GFP and tubulin were used. Images are representative of three independent experiments. (E) Maximum-projection time-lapse images of *mhf2*+, *mhf2*Δ and *bub1*Δ cells expressing Ark1–GFP and mCherry–Atb2. Note that three *mhf2*Δ cells did not exit mitosis (the number of cells observed is shown on the bottom). Scale bars: 10 µm. (F) Plots of the average ('Ave') intensity of Ark1–GFP signals along the spindle at each time point. The number of cells analyzed is indicated. Error bars represent s.d, and *P*-values were calculated by two-way ANOVA. Two independent experiments were performed and similar results were obtained. a.u., arbitrary units.

the lack of attachments between the kinetochores and microtubules (the kinetochores remained relatively immobile). Taken together, our data demonstrate that Mhf2 plays a crucial role in promoting kinetochore–microtubule attachments and faithful chromosome segregation.

DISCUSSION

Faithful chromosome segregation requires proper kinetochore–microtubule attachments and surveillance of the SAC (Musacchio, 2015). Few studies have focused on addressing the roles of CCAN in SAC signaling. In the present work, we demonstrate that the fission yeast CCAN component Mhf2 is involved in regulating chromosome segregation, most likely by promoting SAC signaling and proper attachments between the kinetochores and spindle microtubules (Fig. 6E). Hence, our study delineated the role of the CCAN subcomplex Mhf1–Mhf2 in chromosome segregation.

The molecular architecture of the point centromere or kinetochore has been extensively defined in budding yeast (Akiyoshi et al., 2010; Hinshaw et al., 2019; Yan et al., 2019). Additionally, the molecular architecture of regional centromeres or kinetochores

Journal of Cell Science (2023) 136, jcs260124. doi:10.1242/jcs.260124

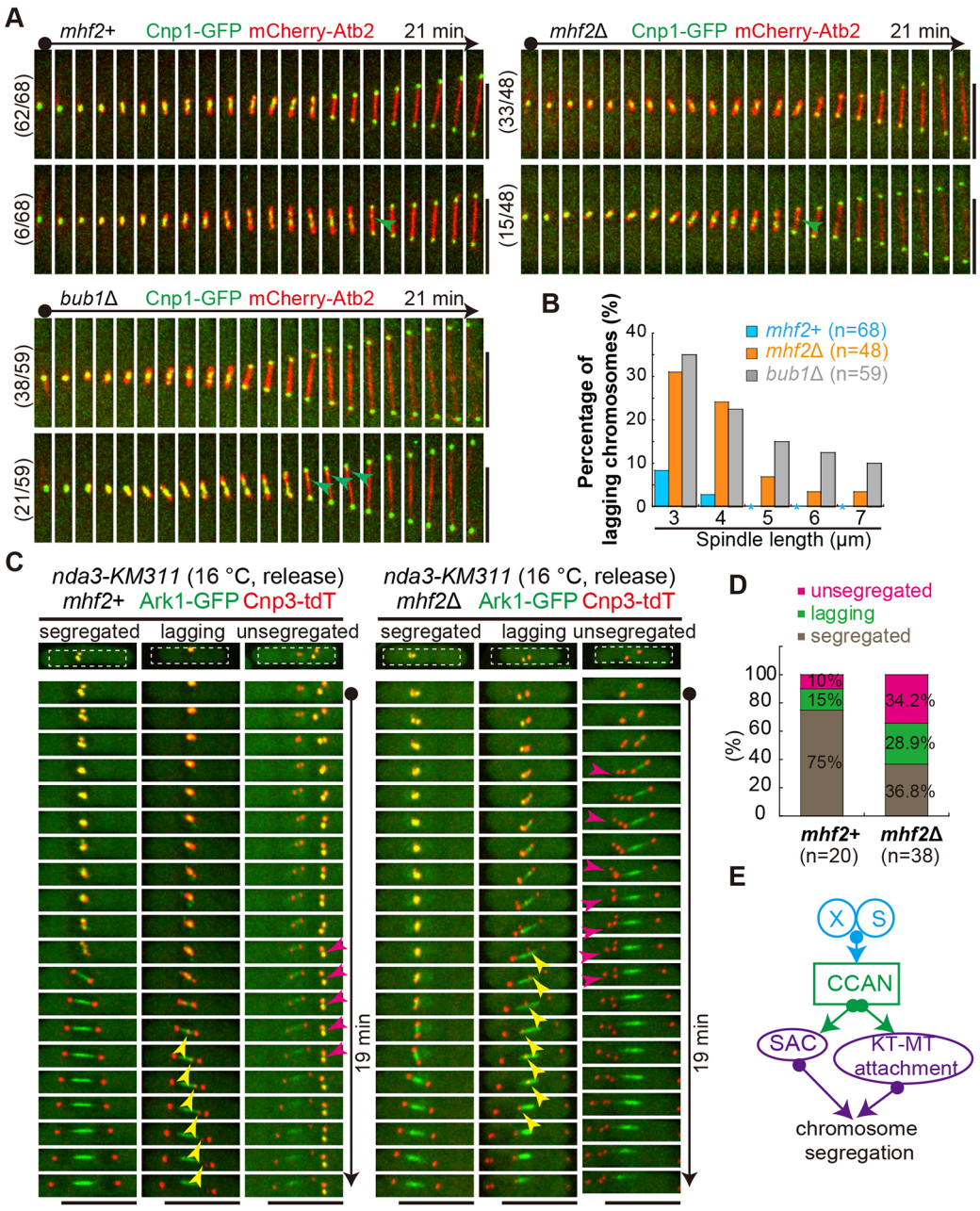

Fig. 6. The absence of Mhf2 causes lagging chromosomes during anaphase and impairs kinetochore–microtubule attachments. (A) Maximum-projection time-lapse images of *mhf2*+, *mhf2*Δ, and *bub1*Δ cells expressing Cnp1–GFP and mCherry–Atb2. Green arrowheads indicate lagging chromosomes. The number of cells analyzed is indicated. Scale bars: 10 µm. (B) Percentage of *mhf2*+, *mhf2*Δ and *bub1*Δ cells displaying lagging chromosomes. Quantification was categorized according to the spindle length (3, 4, 5, 6 and 7 µm). Asterisks indicate no lagging chromosomes. The number of cells analyzed is indicated. (C) Maximum-projection time-lapse images of *mhf2*+ and *mhf2*Δ cells expressing Ark1–GFP and Cnp3–tdTomato and carrying the *nda3-KM311* allele. Cells were cultured at the restrictive temperature of 16°C and then released from the mitotic arrest at 30°C. Three typical types of cells are shown, and each column shows only one cell. At the top of each column, the whole cell is shown and a dashed rectangle indicates the region used to construct the montage images below. Yellow and red arrowheads mark lagging chromosomes and immobile kinetochores, respectively. Scale bars: 10 µm. (D) Quantification of mitotic cells displaying the three typical types of cells indicated in C. The number (*n*) of cells analyzed is indicated. (E) A model illustrating the role of the CCAN complex Mhf1–Mhf2 (CENP-S/X in humans) in chromosome segregation. Mhf1–Mhf2 is required for proper organization of the CCAN complex, which plays a crucial role in promoting the SAC and kinetochore–microtubule (KT–MT) attachments. The absence of Mhf1–Mhf2 impairs the SAC and kinetochore–microtubule attachment, leading to defective chromosome segregation.

in organisms such as fission yeast and human has become clearer (Musacchio and Desai, 2017; Pesenti et al., 2022; Tian et al., 2022; Yatskevich et al., 2022). However, the spatiotemporal order of the assembly of the regional centromere or kinetochore is less defined, as it was postulated that the regional kinetochores of metazoans are likely generated from multiple copies of the CCAN and KMN complexes to project large disk-like structures (Weir et al., 2016).

The fission yeast CCAN subcomplex CENP-S/X (i.e. Mhf1–Mhf2) might play an interdependent role in promoting organization of the CCAN proteinaceous machine, as depletion of Mhf2 attenuates the kinetochore localization of most of the CCAN

Journal of Cell Science

Journal of Cell Science (2023) 136, jcs260124. doi:10.1242/jcs.260124

components except Cnp1 and Cnp20 (Fig. 3). In chicken cells, deletion of CENP-X did not appear to affect the kinetochore localization of CENP-A, CENP-C, CENP-K and CENP-U, and in human cells, CENP-X knockdown did not appear to affect the localization of CENP-H and CENP-O (Amano et al., 2009). This discrepancy could be due mainly to the different experimental conditions used in the previous study and in our work. In this study, all obtained data were based on live-cell imaging and simultaneous analysis of WT and mutant cells in the same images, whereas the previous study was based on immunofluorescence analysis of fixed cells. Therefore, our approach of simultaneous imaging of WT and mutant cells allows for the detection of subtle changes in proteins on kinetochores. Despite the discrepancy, both studies consistently showed that the CCAN subcomplex CENP-S/X is required for promoting proper organization of the KMN network (Fig. 3G, Fig. 4A,C) (Amano et al., 2009). In addition, depletion of CENP-S or CENP-X in chicken cells increased the intra-kinetochore distance, suggesting that the CCAN complex becomes more stretched in CENP-S/X-deficient cells (Amano et al., 2009). It would be of great interest to use spectral image analyses to evaluate whether CENP-S/X is required for the stable localization of CENP-A, CENP-C, CENP-K and CENP-U to the centromeres of human cells.

The CCAN subcomplexes required for the proper localization of Spc7 and Ndc80 to the KMN network in the outer kinetochore were also determined in this study (Fig. 4). Given the crucial role of Mhf2 in promoting the organization of the CCAN complex (Fig. 3), it is conceivable that Mhf2 also regulates the proteins residing in the outer kinetochore (e.g. Spc7, Ndc80 and Bub1) indirectly via the CCAN (Fig. 6E). Indeed, the present work revealed the important role of Mhf2 in regulating the SAC. The altered localization of Bub1 in the absence of Mhf2 might be due to the impaired localization of Spc7 to the kinetochore (Fig. 2F–H) because Mps1-dependent phosphorylation of Spc7 (KNL1 in humans) is responsible for the recruitment of the Bub1–Bub3 complex to the kinetochore (Saurin, 2018). The crucial role of the CCAN component Mhf2 in promoting the SAC is consistent with the previous finding that mutation of the CCAN component Mis6 (CENP-I in humans) impairs the SAC (Shigeaki Saitoh et al., 2005). Mis6 is required for the proper localization of Mad2, but not Bub1, to the kinetochore (Shigeaki Saitoh et al., 2005). By contrast, we found that Mhf2 is required for the proper localization of Bub1 and Mad2 to the kinetochore (Fig. 2B–D; Fig. S3). Despite this finding, how attenuation of the association of Bub1 with kinetochores compromises SAC activity remains to be further investigated in a quantitative manner. Additionally, given that CENP-S/X is not involved in regulating the SAC in chicken cells (Amano et al., 2009), it would be exciting to ascertain whether CENP-S/X is involved in the SAC during human cell division.

The absence of Mhf2 significantly increased the percentage of cells displaying lagging chromosomes (Fig. 6A). This phenotype could not be attributed only to the attenuated SAC function because SAC appeared to be functional in *mhf2*Δ cells (Fig. 1B). The altered localization of the kinase Aurora B/Ark1 to the kinetochore during preanaphase by the absence of Mhf2 (Fig. 5) suggests the possibility that the mechanism for correcting incorrect kinetochore–microtubule attachments is also compromised by the absence of Mhf2. It is well established that Aurora B/Ark1 functions to correct incorrect kinetochore–microtubule attachments during mitosis by phosphorylating Ndc80 (Welburn et al., 2010). Interestingly, our data showed that Aurora B/Ark1 could either delocalize from the kinetochores or localize more strongly to the kinetochores (Fig. 5). Given the crucial role of Aurora B-mediated phosphorylation of Ndc80 in reducing the affinity of Ndc80 to microtubules, either case of the altered localization of Aurora B/Ark1 might risk improper attachments of the kinetochores to spindle microtubules and consequently result in defective chromosome segregation. As the absence of Mhf2 affects multiple components in the kinetochore to varying degrees (Fig. 3H), it would be interesting to determine how the altered kinetochore components, alone or collectively, cause mitotic defects. Future work will be directed to delineate the causal effect of Mhf2 in CCAN integrity and SAC signaling given the recently solved cryo-electron microscopy structure of the human CCAN (Pesenti et al., 2022; Tian et al., 2022; Yatskevich et al., 2022).

In summary, our delineation of the CENP-S/X homologs in fission yeast revealed their uncharacterized functions in regional centromere plasticity and the SAC.

MATERIALS AND METHODS

Yeast strains

Yeast genetics were performed as previously described (Forsburg and Rhind, 2006) and *S. pombe* strains were constructed by either random spore digestion or tetrad dissection. Gene deletion and tagging were performed by PCR-based methods using the pFA6a series of plasmids, and yeast transformation was carried out by the lithium acetate method (Forsburg and Rhind, 2006). The strains used in this study are listed in Table S1.

Microscopy

Imaging experiments were carried out with a PerkinElmer UltraVIEW VoX spinning-disk microscope equipped with a Hamamatsu C9100-23B EMCCD camera and a CFI Apochromat TIRF 100× objective (NA=1.49). For live-cell imaging, yeast strains were inoculated into Edinburgh minimal medium with five supplements (adenine, leucine, uracil, histidine and lysine; 0.225 g/l each; referred to as EMM5S) (Formedium), unless specified otherwise. The *nda3-KM311* cells were inoculated into rich yeast extract medium (YE) with the same five supplements (referred to as YE5S) (Formedium) and, before microscopy analysis, the *nda3-KM311* cells were treated at 16°C for 6 h until the optical density at 600 nm (OD600) reached 0.5–1.0. The temperature-sensitive mutant strains (in Fig. 4) were cultured in YE5S medium for 2 h before analysis by microscopy. To prepare live-cell microscopy slides, the corresponding medium containing 3% agar was solidified on a glass slide and 0.5 µl of cells were placed on top of the agar and covered with a coverslip. Imaging was performed at room temperature. Stack images containing 11 planes with a spacing of 0.5 µm were acquired and time-lapse images were taken every 1 min (500 ms exposure for GFP and tdTomato).

MitoTracker and lectin staining

To stain WT cells, we used MitoTracker Red or Green (Invitrogen, M7512 and M7514) and lectin (Sigma-Aldrich, L9381 and L5264). Briefly, cells were grown in EMM5S until the log phase was reached and MitoTracker (storage concentration, 10 mM; dilution factor, 1:300) was then added into the cell culture. The cells were treated in the dark for 10 min and then centrifuged and washed with EMM5S two times. Lectin was used at a final concentration of 100 µg/ml and the staining procedure was the same as that used for MitoTracker staining.

Data analysis

Imaging data were analysed with MetaMorph (Molecular Devices) and ImageJ 1.52 (National Institutes of Health). To measure the intensity of Bub1–GFP in Fig. 1B and Ark1–GFP in Fig. 5F, line-scan intensity analysis was performed to obtain a plot of the signal intensity against time for each cell by MetaMorph 7.7. Graph and statistical analyses were performed with KaleidaGraph 4.5 (Synergy) and the illustration diagram was generated with Adobe Illustrator.

Immunoprecipitation and western blotting

For the immunoprecipitation assay, *mhf2*+ and *mhf2*Δ cells carrying the *nda3-KM311* allele were treated at 16°C for 6 h until the OD600 reached

0.8–1.0. The collected cells were ground with an RM200 mortar grinder (Retsch) after being frozen in liquid nitrogen. Cleaned cell lysates in TBS with 0.1% Triton X-100 were incubated with anti-GFP antibody (homemade, validated using strains expressing GFP fusion proteins; GeneScript; 5 µg)-bound Dynabeads (protein G beads; Invitrogen) at 4°C for 2 h, followed by washing with TBS with 0.1% Triton X-100 buffer four times and 1× TBS buffer once. The immunoprecipitated products were analyzed by western blotting using an anti-GFP antibody (Rockland Immunochemicals, 600-101-215; 1:2000) and horseradish peroxidase-conjugated anti-goat IgG (Abclonal, AS029, 1:10,000).

For analysis of protein expression, whole-cell protein extracts were prepared by the trichloroacetic acid (TCA) method (Forsburg and Rhind, 2006), followed by SDS-PAGE analysis. Briefly, cells were collected and washed with 1 ml distilled deionized water. The collected cells were resuspended with 50 µl 20% TCA (URChem, 81606) and mixed by vortexing. Approximately 200 µl glass beads (BioSpec, 11079105) were added and the cells were disrupted using a Retsch MM 400 laboratory mill, followed by addition of 50 µl 20% TCA to the cell lysates. The lysates were then vortexed and an additional 400 µl of 5% TCA was added. After removing the glass beads, the samples were centrifuged at 16,000 ***g*** for 10 min at 4°C to remove the supernatant. Finally, the precipitate was resuspended in 100 µl 1× SDS sample buffer and 25 µl 1.5 M Tris-HCl pH 8.0, followed by boiling at 100°C for 5 min. The proteins were analyzed by western blotting with anti-GFP (Rockland, 600-101-215; 1:2000) and anti-tubulin (BioAcademia, 63-160; 1:10,000) antibodies, and horseradish peroxidase-conjugated anti-rabbit IgG (Bio-Rad, 170-546, 1:10,000). The original western blots corresponding to the cropped images shown in the main and supplementary figures are included Fig. S5.

RT-qPCR

To evaluate the expression of the neighboring genes of *mhf2*, RT-qPCR was performed. Briefly, total RNA was extracted from cells cultured in YE5S with a genomic DNA purification kit (ZymoResearch, R1002), and cDNA was generated by reverse transcription PCR with a HiScript III RT SuperMix kit (Vazyme, R323-01). Finally, quantitative PCR was performed by using a AceQ qPCR SYBR Green Master Mix kit (Vazyme, Q111-02/03) on a LightCycle 96 instrument (Roche). Three independent experiments were carried out.

Acknowledgements

We thank Takashi Toda (Cancer Research UK, London, UK) and Dr Phong Tran (University of Pennsylvania) for providing yeast strains. We also thank members of the Fu Laboratory for helpful discussions.

Competing interests

The authors declare no competing or financial interests.

Author contributions

Conceptualization: C.F.; Methodology: Y. Jian; Formal analysis: Y. Jian; Investigation: Y. Jian, L.N., S.L., Y. Jiang, Z.D., X.L.; Writing - original draft: Y. Jian, X.L., X.Y., C.F.; Writing - review & editing: C.F.; Supervision: X.Y., C.F.; Funding acquisition: C.F.

Funding

This work is supported by grants from the National Key Research and Development Program of China (2022YFA1303100) and the National Natural Science Foundation of China (32070707 and 31871350 to C.F., and 31621002).

Data availability

All relevant data can be found within the article and its supplementary information.

Peer review history

The peer review history is available online at https://journals.biologists.com/jcs/article-lookup/doi/10.1242/jcs.260142.reviewer-comments.pdf

References

Akiyoshi, B., Sarangapani, K. K., Powers, A. F., Nelson, C. R., Reichow, S. L., Arellano-Santoyo, H., Gonen, T., Ranish, J. A., Asbury, C. L. and Biggins, S. (2010). Tension directly stabilizes reconstituted kinetochore-microtubule attachments. *Nature* **468**, 576-579. doi:10.1038/nature09594

Amano, M., Suzuki, A., Hori, T., Backer, C., Okawa, K., Cheeseman, I. M. and Fukagawa, T. (2009). The CENP-S complex is essential for the stable assembly of outer kinetochore structure. *J. Cell Biol.* **186**, 173-182. doi:10.1083/jcb.200903100

Cheeseman, I. M. (2014). The kinetochore. *Cold Spring Harb. Perspect Biol.* **6**, a015826. doi:10.1101/cshperspect.a015826

Cheeseman, I. M., Chappie, J. S., Wilson-Kubalek, E. M. and Desai, A. (2006). The conserved KMN network constitutes the core microtubule-binding site of the kinetochore. *Cell* **127**, 983-997. doi:10.1016/j.cell.2006.09.039

DeLuca, J. G., Dong, Y., Hergert, P., Strauss, J., Hickey, J. M., Salmon, E. D. and McEwen, B. F. (2005). Hec1 and nuf2 are core components of the kinetochore outer plate essential for organizing microtubule attachment sites. *Mol. Biol. Cell* **16**, 519-531. doi:10.1091/mbc.e04-09-0852

Ding, M., Jiang, J., Yang, F., Zheng, F., Fang, J., Wang, Q., Wang, J., Yao, W., Liu, X., Gao, X. et al. (2019). Holliday junction recognition protein interacts with and specifies the centromeric assembly of CENP-T. *J. Biol. Chem.* **294**, 968-980. doi:10.1074/jbc.RA118.004688

Fischer, E. S., Yu, C. W. H., Bellini, D., McLaughlin, S. H., Orr, C. M., Wagner, A., Freund, S. M. V. and Barford, D. (2021). Molecular mechanism of Mad1 kinetochore targeting by phosphorylated Bub1. *EMBO Rep.* **22**, e52242. doi:10.15252/embr.202052242

Forsburg, S. L. and Rhind, N. (2006). Basic methods for fission yeast. *Yeast* **23**, 173-183. doi:10.1002/yea.1347

Hagan, I. M., Grallert, A. and Simanis, V. (2016). Synchronizing progression of schizosaccharomyces pombe cells from prophase through mitosis and into S Phase with nda3-KM311 arrest release. *Cold Spring Harb. Protoc* **2016**, 711-715. doi:10.1101/pdb.prot091256

Hara, M. and Fukagawa, T. (2017). Critical foundation of the kinetochore: the constitutive centromere-associated network (CCAN). *Prog. Mol. Subcell. Biol.* **56**, 29-57. doi:10.1007/978-3-319-58592-5_2

Hayles, J. and Nurse, P. (2018). Introduction to fission yeast as a model system. *Cold Spring Harb Protoc.* **2018**, 323-333. doi:10.1101/pdb.top079749

Hinshaw, S. M., Dates, A. N. and Harrison, S. C. (2019). The structure of the yeast Ctf3 complex. *Elife* **8**, e48215. doi:10.7554/eLife.48215

Hiraoka, Y., Toda, T. and Yanagida, M. (1984). The NDA3 gene of fission yeast encodes beta-tubulin: a cold-sensitive nda3 mutation reversibly blocks spindle formation and chromosome movement in mitosis. *Cell* **39**, 349-358. doi:10.1016/0092-8674(84)90013-8

Hori, T., Shang, W.-H., Takeuchi, K. and Fukagawa, T. (2013). The CCAN recruits CENP-A to the centromere and forms the structural core for kinetochore assembly. *J. Cell Biol.* **200**, 45-60. doi:10.1083/jcb.201210106

Hori, T., Kagawa, N., Toyoda, A., Fujiyama, A., Misu, S., Monma, N., Makino, F., Ikeo, K. and Fukagawa, T. (2017). Constitutive centromere-associated network controls centromere drift in vertebrate cells. *J. Cell Biol.* **216**, 101-113. doi:10.1083/jcb.201605001

Huis In 't Veld, P. J., Jeganathan, S., Petrovic, A., Singh, P., John, J., Krenn, V., Weissmann, F., Bange, T. and Musacchio, A. (2016). Molecular basis of outer kinetochore assembly on CENP-T. *Elife* **5**, e21007. doi:10.7554/eLife.21007

Liang, C., Zhang, Z., Chen, Q., Yan, H., Zhang, M., Zhou, L., Xu, J., Lu, W. and Wang, F. (2020). Centromere-localized Aurora B kinase is required for the fidelity of chromosome segregation. *J. Cell Biol.* **219**, e201907092. doi:10.1083/jcb.201907092

Liu, S. T., Hittle, J. C., Jablonski, S. A., Campbell, M. S., Yoda, K. and Yen, T. J. (2003). Human CENP-I specifies localization of CENP-F, MAD1 and MAD2 to kinetochores and is essential for mitosis. *Nat. Cell Biol.* **5**, 341-345. doi:10.1038/ncb953

Liu, H., Qu, Q., Warrington, R., Rice, A., Cheng, N. and Yu, H. (2015). Mitotic transcription installs Sgo1 at centromeres to coordinate chromosome segregation. *Mol. Cell* **59**, 426-436. doi:10.1016/j.molcel.2015.06.018

London, N. and Biggins, S. (2014). Signalling dynamics in the spindle checkpoint response. *Nat. Rev. Mol. Cell Biol.* **15**, 736-747. doi:10.1038/nrm3888

Lu, M. and He, X. (2019). Centromere repositioning causes inversion of meiosis and generates a reproductive barrier. *Proc. Natl. Acad. Sci. USA* **116**, 21580-21591. doi:10.1073/pnas.1911745116

Mulvihill, D. P., Petersen, J., Ohkura, H., Glover, D. M. and Hagan, I. M. (1999). Plo1 kinase recruitment to the spindle pole body and its role in cell division in Schizosaccharomyces pombe. *Mol. Biol. Cell* **10**, 2771-2785. doi:10.1091/mbc.10.8.2771

Musacchio, A. (2015). The molecular biology of spindle assembly checkpoint signaling dynamics. *Curr. Biol.* **25**, R1002-R1018. doi:10.1016/j.cub.2015.08.051

Musacchio, A. and Desai, A. (2017). A molecular view of kinetochore assembly and function. *Biology (Basel)* **6**, 5. doi:10.3390/biology6010005

Nishino, T., Takeuchi, K., Gascoigne, K. E., Suzuki, A., Hori, T., Oyama, T., Morikawa, K., Cheeseman, I. M. and Fukagawa, T. (2012). CENP-T-W-S-X forms a unique centromeric chromatin structure with a histone-like fold. *Cell* **148**, 487-501. doi:10.1016/j.cell.2011.11.061

Perpelescu, M. and Fukagawa, T. (2011). The ABCs of CENPs. *Chromosoma* **120**, 425-446. doi:10.1007/s00412-011-0330-0

Pesenti, M. E., Prumbaum, D., Auckland, P., Smith, C. M., Faesen, A. C., Petrovic, A., Erent, M., Maffini, S., Pentakota, S., Weir, J. R. et al. (2018).

Reconstitution of a 26-subunit human kinetochore reveals cooperative microtubule binding by CENP-OPQUR and NDC80. *Mol. Cell* **71**, 923-939.e10. doi:10.1016/j.molcel.2018.07.038

Pesenti, M. E., Raisch, T., Conti, D., Walstein, K., Hoffmann, I., Vogt, D., Prumbaum, D., Vetter, I. R., Raunser, S. and Musacchio, A. (2022). Structure of the human inner kinetochore CCAN complex and its significance for human centromere organization. *Mol. Cell* **82**, 2113-2131.e8. doi:10.1016/j.molcel.2022.04.027

Petersen, J., Paris, J., Willer, M., Philippe, M. and Hagan, I. M. (2001). The S. pombe aurora-related kinase Ark1 associates with mitotic structures in a stage dependent manner and is required for chromosome segregation. *J. Cell Sci.* **114**, 4371-4384. doi:10.1242/jcs.114.24.4371

Rago, F., Gascoigne, K. E. and Cheeseman, I. M. (2015). Distinct organization and regulation of the outer kinetochore KMN network downstream of CENP-C and CENP-T. *Curr. Biol.* **25**, 671-677. doi:10.1016/j.cub.2015.01.059

Saitoh, S., Ishii, K., Kobayashi, Y. and Takahashi, K. (2005). Spindle checkpoint signaling requires the mis6 kinetochore subcomplex, which interacts with mad2 and mitotic spindles. *Mol. Biol. Cell* **16**, 3666-3677. doi:10.1091/mbc.e05-01-0014

Saurin, A. T. (2018). Kinase and phosphatase cross-talk at the kinetochore. *Front. Cell Dev. Biol.* **6**, 62. doi:10.3389/fcell.2018.00062

Sharp-Baker, H. and Chen, R. H. (2001). Spindle checkpoint protein Bub1 is required for kinetochore localization of Mad1, Mad2, Bub3, and CENP-E, independently of its kinase activity. *J. Cell Biol.* **153**, 1239-1250. doi:10.1083/jcb.153.6.1239

Shigeaki Saitoh, K. I., Yasuyo, K. and Kohta, T. (2005). Spindle checkpoint signaling requires the mis6 kinetochore subcomplex, which interacts with Mad2 and mitotic spindles. *Mol. Biol. Cell* **16**, 3666-3677. doi:10.1091/mbc.e05-01-0014

Tao, Y., Jin, C., Li, X., Qi, S., Chu, L., Niu, L., Yao, X. and Teng, M. (2012). The structure of the FANCM-MHF complex reveals physical features for functional assembly. *Nat. Commun.* **3**, 782. doi:10.1038/ncomms1779

Tian, T., Chen, L., Dou, Z., Yang, Z., Gao, X., Yuan, X., Wang, C., Liu, R., Shen, Z., Gui, P. et al. (2022). Structural insights into human CCAN complex assembled onto DNA. *Cell Discov* **8**, 90. doi:10.1038/s41421-022-00439-6

Watanabe, Y. (2010). Temporal and spatial regulation of targeting aurora B to the inner centromere. *Cold Spring Harb. Symp. Quant. Biol.* **75**, 419-423. doi:10.1101/sqb.2010.75.035

Weir, J. R., Faesen, A. C., Klare, K., Petrovic, A., Basilico, F., Fischbock, J., Pentakota, S., Keller, J., Pesenti, M. E., Pan, D. et al. (2016). Insights from biochemical reconstitution into the architecture of human kinetochores. *Nature* **537**, 249-253. doi:10.1038/nature19333

Welburn, J. P., Vleugel, M., Liu, D., Yates, J. R., III, Lampson, M. A., Fukagawa, T. and Cheeseman, I. M. (2010). Aurora B phosphorylates spatially distinct targets to differentially regulate the kinetochore-microtubule interface. *Mol. Cell* **38**, 383-392. doi:10.1016/j.molcel.2010.02.034

Yamagishi, Y., Honda, T., Tanno, Y. and Watanabe, Y. (2010). Two histone marks establish the inner centromere and chromosome bi-orientation. *Science* **330**, 239-243. doi:10.1126/science.1194498

Yamagishi, Y., Yang, C. H., Tanno, Y. and Watanabe, Y. (2012). MPS1/Mph1 phosphorylates the kinetochore protein KNL1/Spc7 to recruit SAC components. *Nat. Cell Biol.* **14**, 746-752. doi:10.1038/ncb2515

Yan, Z., Delannoy, M., Ling, C., Daee, D., Osman, F., Muniandy, P. A., Shen, X., Oostra, A. B., Du, H., Steltenpool, J. et al. (2010). A histone-fold complex and FANCM form a conserved DNA-remodeling complex to maintain genome stability. *Mol. Cell* **37**, 865-878. doi:10.1016/j.molcel.2010.01.039

Yan, K., Yang, J., Zhang, Z., McLaughlin, S. H., Chang, L., Fasci, D., Ehrenhofer-Murray, A. E., Heck, A. J. R. and Barford, D. (2019). Structure of the inner kinetochore CCAN complex assembled onto a centromeric nucleosome. *Nature* **574**, 278-282. doi:10.1038/s41586-019-1609-1

Yatskevich, S., Muir, K. W., Bellini, D., Zhang, Z., Yang, J., Tischer, T., Predin, M., Dendooven, T., McLaughlin, S. H. and Barford, D. (2022). Structure of the human inner kinetochore bound to a centromeric CENP-A nucleosome. *Science* **376**, 844-852. doi:10.1126/science.abn3810